SI Appendix

Decoupling Redox Actives Solubility and Energy Density in Redox Flow Batteries Using Supersaturated, Phase-change Electrolytes

Jing Xie[a], Shrihari Sankarasubramanian[b,c], Jeffrey G. Catalano[d], Vijay Ramani*[a]

[a]Department of Energy, Environmental & Chemical Engineering, Washington University in St. Louis, St. Louis, MO 63130; [b]Department of Biomedical Engineering and Chemical Engineering, University of Texas at San Antonio, San Antonio, TX 78429; [c]Department of Mechanical, Aerospace and Industrial Engineering, University of Texas at San Antonio, San Antonio, TX 78429; [d]Department of Earth and Planetary Sciences, Washington University in St. Louis, St. Louis, MO 63130.

*Corresponding author: Vijay Ramani; 1 Brookings Drive, South Brookings Hall, Room 135, St. Louis, MO 63130; 314-935-7924; ramani@wustl.edu

S1. Materials and Methods

S1.1. Materials Characterization

Scanning electron microscope and energy dispersive X-ray (SEM/EDX) was conducted with Thermofisher Quattro S ESEM coupled with an Oxford AzTec Energy Dispersive X-Ray Spectrometer. The acceleration voltage was 5 kV and the working distance between the bottom of bottom and sample surface was around 10 mm. The weight of carbon felt (CF) was measured with an analytical and precision balance (VWR-64B). For the raw CF, the measurement was conducted after it was dried at 60 °C in the oven for 24 h; for the CF after RFB test, it was rinsed with DI water carefully first followed by the drying and measurement.

S1.2. RFBs test

The flow field was a serpentine type with enlarged inlet and outlet, as shown in Fig. S1. For the constant-current charge/discharge, a current density of ±50 mA/cm^2 was applied until the potential reached the cut-off value (2 or 1 V); for the following constant-voltage charge/discharge, a voltage of 2 or 1 V was applied until the current density reached the cut-off value (±20 mA/cm^2). The purpose of the constant-voltage phase was to help the system fully charge/discharge. As mentioned in the main text, a short constant-voltage stage was applied at the beginning for 2 mins, which typically was terminated by the duration instead of cut-off condition.

S2. Results and Discussion

S2.1. Speciation in sulfuric acid (H_2SO_4)

In H_2SO_4, the dissociation of protons is governed by the protonation equilibrium as follows:

$$H_2SO_4 \leftrightarrow HSO_4^- + H^+ \quad pK_1 = -3 \qquad [1]$$

$$HSO_4^- \leftrightarrow SO_4^{2-} + H^+ \quad pK_2 = 1.99 \qquad [2]$$

where pK equals to -log(K). The very small pK_1 value suggests that equation (1) could be assumed to proceed to completion. Based on this, the abundance of bisulfate (HSO_4^-) and sulfate (SO_4^{2-}) as a function of pH was plotted as shown in Fig. S4. In low pH (< 0) environment, HSO_4^- is the dominant species; as it becomes more neutral, SO_4^{2-} gradually takes precedence.

S2.2. Speciation of ammonium (NH_4^+) and ammonia (NH_3)

The dissociation of proton in NH_4^+ is governed by the following equilibrium:

$$NH_4^+ \leftrightarrow NH_3 + H^+ \quad pK_a = 9.24 \qquad [3]$$

Similar as the abundance of HSO_4^- and SO_4^{2-} in S2.1, when the system pH equals to pK_a, the amount of conjugate acid and base is the same. Since the pH of all solutions in our study was considerably lower than 9.24, it is reasonable to ignore the proton release from NH_4^+.

S2.3. Speciation of cerium(IV) hydrolysis

Four different Ce(IV) hydrolysis was considered as follows:

$$Ce^{4+} + H_2O \leftrightarrow Ce(OH)^{3+} + H^+ \quad logK_1 = 0.764 \qquad [4]$$

$$Ce^{4+} + 2H_2O \leftrightarrow Ce(OH)_2^{2+} + 2H^+ \quad logK_2 = 0.048 \qquad [5]$$

$$Ce^{4+} + 3H_2O \leftrightarrow Ce(OH)_3^+ + 3H^+ \quad logK_3 = -1.485 \qquad [6]$$

$$Ce^{4+} + 4H_2O \leftrightarrow Ce(OH)_4^0 + 4H^+ \quad logK_4 = -4.124 \qquad [7]$$

The equilibrium constants were taken from previous literature (1, 2). In an ideal case in which no other complexation of anions is present, the fraction of different Ce(IV) species was calculated based on mass balance principle, shown as follows:

$$[Ce^{4+}] = \frac{1}{1 + \frac{K_1}{[H^+]} + \frac{K_2}{[H^+]^2} + \frac{K_3}{[H^+]^3} + \frac{K_4}{[H^+]^4}} \qquad [8]$$

$$[Ce(OH)^{3+}] = \frac{K_1}{[H^+]} \times [Ce^{4+}] \qquad [9]$$

$$\left[Ce(OH)_2^{2+}\right] = \frac{K_2}{[H^+]^2} \times [Ce^{4+}] \quad [10]$$

$$\left[Ce(OH)_3^{+}\right] = \frac{K_3}{[H^+]^3} \times [Ce^{4+}] \quad [11]$$

$$\left[Ce(OH)_4^{0}\right] = \frac{K_4}{[H^+]^4} \times [Ce^{4+}] \quad [12]$$

The corresponding speciation curve is depicted in Fig. S5.

S2.4 Deconvolution of Raman spectra in OH stretching region

As polar molecule, the oxygen atom in a water molecule is negatively charged, and the two hydrogen atoms are positively charged. Thus, the oxygen atom is considered as an acceptor, and the hydrogen atom is a donor. Based on the different number and location of hydrogen bond formed in a water molecule, the hydrogen bond is classified into five categories: single donor-double acceptor (DAA, 3004 cm^{-1}), double donor-double acceptor (DDAA, 3227 cm^{-1}), single donor-single acceptor (DA, 3431 cm^{-1}), double donor-single acceptor (DDA, 3565 cm^{-1}), and free OH vibrations (3633 cm^{-1}) (3). The deconvoluted spectra are displayed in Fig. S6.

S2.5 Theoretical calculation

S2.5.1 0.123 M $Ce(SO_4)_2$ in water

The *pH* decreased from 7 (water) to 0.7 after dissolution, and all acidity came from Ce(IV) hydrolysis. Besides, we assume that sulfate species was in HSO_4^-. The concentration of total protons was:

$$TOT\ H^+ = TOT\ SO_4 + 10^{-pH} = 0.123 \times 2 + 10^{-0.7} = 0.4455\ M \quad [13]$$

the ratio between total protons and Ce(IV) was:

$$\frac{TOT\ H^+}{TOT\ Ce(IV)} = \frac{0.4455}{0.123} = 3.62 \approx 3.5 \quad [14]$$

The result indicates that for each Ce(IV), 3.5 protons were released from hydrolysis. Thus, it is proposed that the dominant hydrolysis reactions were equations (6) and (7).

S2.5.2 0.123 M $Ce(SO_4)_2$ in 1.05 M H_2SO_4

The *pH* decreased from -0.12 (H_2SO_4) to -0.19 after dissolution, and the acidity came from both H_2SO_4 and Ce(IV). Due to the extremely low *pH* value, H_2SO_4 would only undergo the first deprotonation completely, and all sulfate species was in HSO_4^-. The concentration of protons released by Ce(IV) was calculated as follows:

$$TOT\ H^+\ by\ Ce(IV) = TOT\ SO_4\ from\ Ce(SO_4)_2 + 10^{-pH2} - 10^{-pH1}$$

$$= 0.123 \times 2 + 10^{0.19} - 10^{0.12} = 0.4766\ M \qquad [15]$$

where the first term represents the protons required to protonate SO_4^{2-} from $Ce(SO_4)_2$, and the rest reveal the *pH* change. The ratio between protons released by Ce(IV) and Ce(IV) concentration was calculated by

$$\frac{TOT\ H^+\ by\ Ce(IV)}{TOT\ Ce(IV)} = \frac{0.4766}{0.123} = 3.87 \approx 4 \qquad [16]$$

This result suggests that the main hydrolysis reaction was equation (7). Combined with the fact that the stable structure of Ce(IV) and sulfate complex is achieved when Ce:HSO_4^- is 1:3 (4), we propose that the Ce(IV) structure in our study was $[Ce(OH)_4(HSO_4^-)_3]^{3-}$. This is slightly different from the structure reported previously (4), and the reason is explained in the main text: the Ce(IV) concentration used in previous study was exceptionally low.

S2.5.3 0.123 M $Ce(SO_4)_2$ in 1.05 M AS

The *pH* decreased from 5.4 (AS) to 1.63 after dissolution. While all acidity came from Ce(IV) hydrolysis, sulfate species was in both HSO_4^- and SO_4^{2-} since the *pH* was close to pK_2 of H_2SO_4. It is again assumed that Ce:HSO_4^- was 1:3 in complex, thus the concentration of free sulfate species was calculated as follows:

$$Free\ SO_4 = 1.05 + 0.123 \times 2 - 0.123 \times 3 = 0.927\ M \quad [17]$$

where the first and second term represent sulfate species from AS and $Ce(SO_4)_2$, respectively, and the third term represents the sulfate species bound with Ce(IV). Next, according to the second deprotonation equilibrium of H_2SO_4, the concentration of HSO_4^- and SO_4^{2-} obeys the following relationship:

$$\frac{[SO^{2-}_4][H^+]}{[HSO^-_4]} = 10^{-1.99} \quad [18]$$

from which the concentration of free in solution was calculated by

$$Free\ HSO^-_4 = 0.927 \times \frac{2.29}{2.29 + 1} = 0.6452\ M \quad [19]$$

Then the amount of total protons was

$$TOT\ H^+ = free\ HSO^-_4 + HSO^-_4\ complexed\ with\ Ce(IV) + pH$$

$$= 0.6452 + 0.123 \times 3 + 10^{-1.63} = 1.038\ M \quad [20]$$

The ratio between protons released by Ce(IV) and Ce(IV) concentration was then calculated as

$$\frac{TOT\ H^+}{TOT\ Ce(IV)} = \frac{1.038}{0.123} = 8.45 \approx 8 \quad [21]$$

This suggests that about eight protons were required for the dissolution of each Ce(IV). According to our analysis above, however, the highest number of protons released from water hydrolysis was four. Given this result, we propose a new Ce(IV) hydrolysis process in this case which incorporates NH_4^+ as follows:

$$Ce^{4+} + 4H_2O + 4NH^+_4 \leftrightarrow Ce(OH)_4(NH_3)^0_4 + 8H^+ \quad [22]$$

S2.5.4 Diffusion coefficient (D_0) and standard rate constant (k_0)

Since the electron transfer coefficient, α, was calculated manually according to equation 7 in the main text, the Nicholson-Shain (N-S) and Klingler-Kochi (K-K) equations were modified by moving the α term to the left-hand side as follows.

For N-S:

$$\frac{i_p}{\alpha^{\frac{1}{2}}} = (2.99 \times 10^5) n^{3/2} A C_0 D_0^{1/2} \nu^{1/2} \quad [23]$$

For K-K equation, by defining χ:

$$\chi = \exp\left[\frac{\alpha n F}{RT}|E_p - E_0|\right] / \alpha^{1/2} \quad [24]$$

then

$$\chi = \frac{2.18}{k_0}\left[\frac{D_0 n F}{RT}\right]^{1/2} \nu^{1/2} \quad [25]$$

$i_p/\alpha^{0.5}$ vs. $\nu^{0.5}$ and χ vs. $\nu^{0.5}$ were plotted to obtain N-S and K-K plot, respectively, as shown in Fig. S7. The slopes of new N-S and K-K plots were used to calculate the value of D_0 and k_0 and the results are tabulated in table S6.

S2.6 Ti-Ce RFBs test

S2.6.1 Single charge of V-Ti RFB

To transfer the original Ti(IV) electrolyte into Ti(III), vanadium(V) oxysulfate was dissolved into AS and paired with Ti(IV) to form a V-Ti RFB. The charge process was used to reduce Ti(IV) into Ti(III) based on the following reaction:

$$V(IV) + Ti(IV) \rightarrow V(V) + Ti(III) \quad [26]$$

The concentration and volume of both V(IV) and Ti(IV) was 1.23 M and 50 mL, respectively. The theoretical time required for a full charge could be calculated as follows:

$$Time = \frac{CVF}{iA} \quad [27]$$

where C is concentration (1.23 M), V is electrolyte volume (0.05 L), F is Faraday constant (96485 C/mol), i is current density (50 mA/cm^2), and A is electrode surface area (25 cm^2). The theoretical charge time is calculated as 1.32 h, and the actual experimental time was 1.2 h when the high frequency resistance (HFR) was raised to a very high level due to the deposition of V on the membrane surface, as shown in Fig. S10.

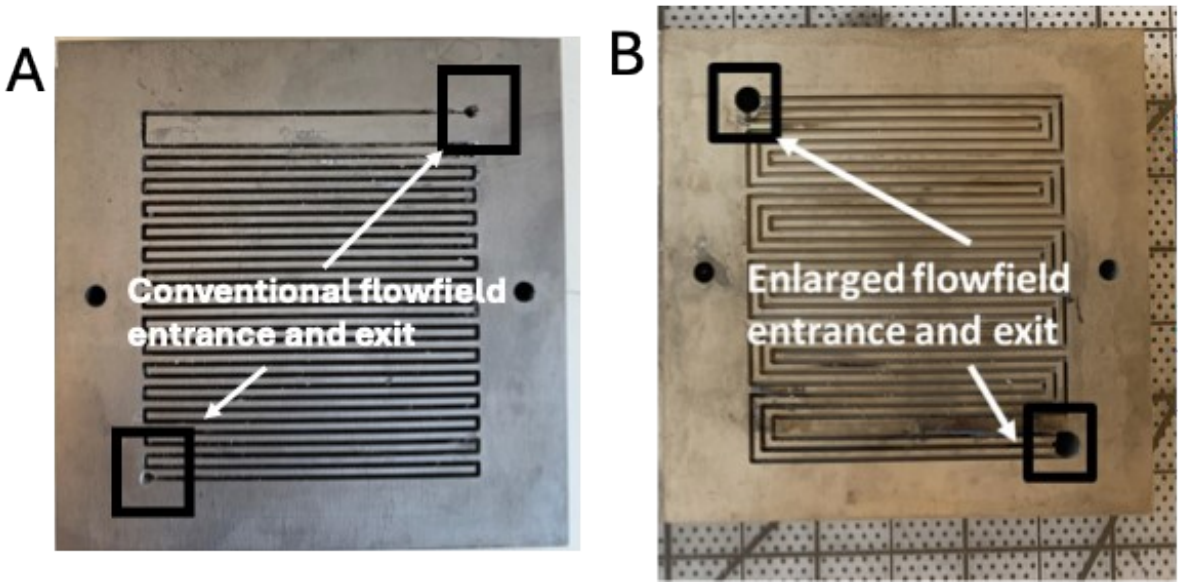

147

148 **Figure S1.** Serpentine flow field with conventional (A) and enlarged (B) entrance and exit.

149

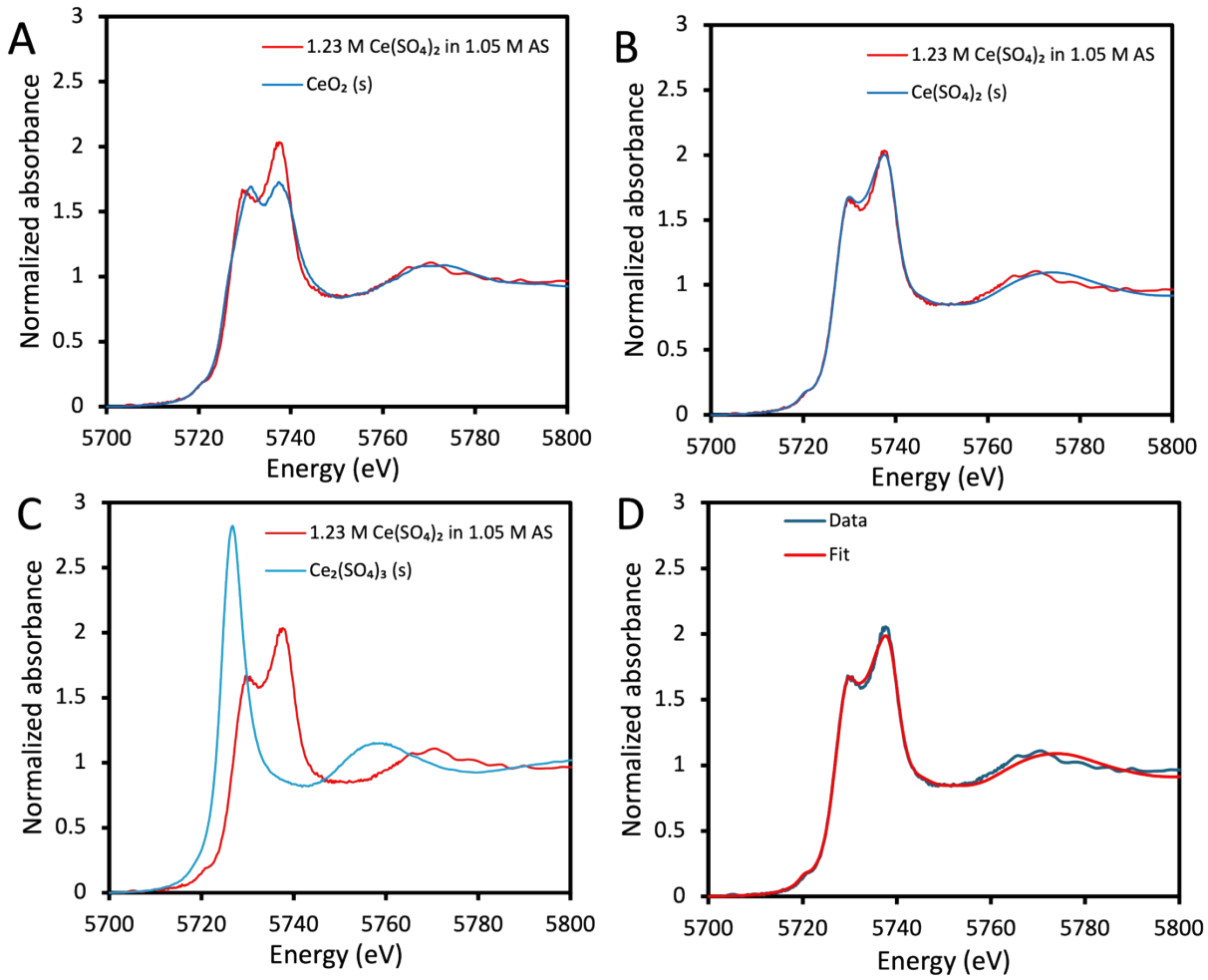

Figure S2. Comparison of the Ce L_{III}-edge XANES spectrum of 1.23 M $Ce(SO_4)_2$ in 1.05 M AS solution with the solid phase of (A) CeO_2, (B) $Ce(SO_4)_2$, and (C) $Ce_2(SO_4)_3$. (D) Linear-combination fit of the Ce L_{III}-edge XANES spectrum of 1.23 M $Ce(SO_4)_2$ in 1.05 M AS solution with the spectra of $Ce(SO_4)_2$ and $Ce_2(SO_4)_3$ standards.

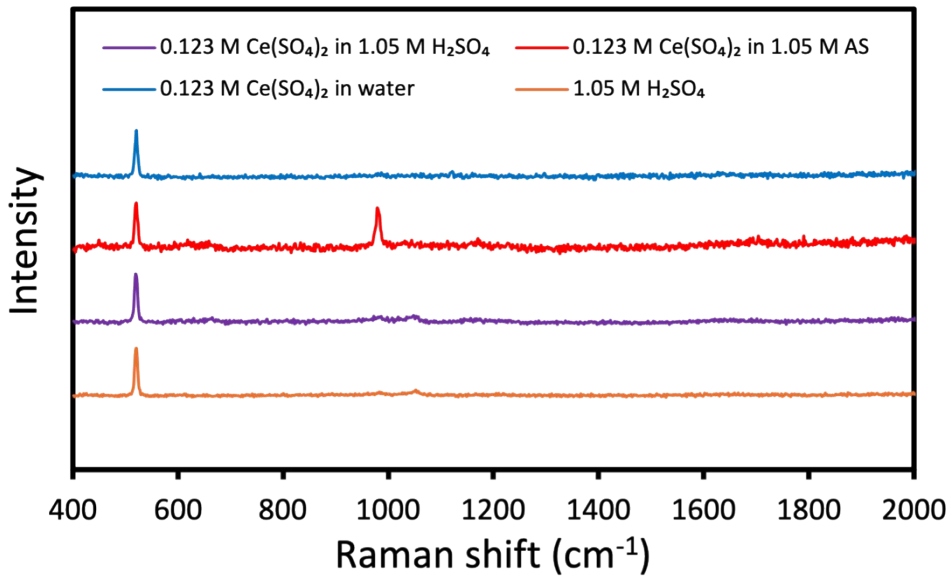

156

157 **Figure S3.** Low-frequency Raman spectra of a fixed concentration of $Ce(SO_4)_2$ in different
158 supporting electrolytes.
159

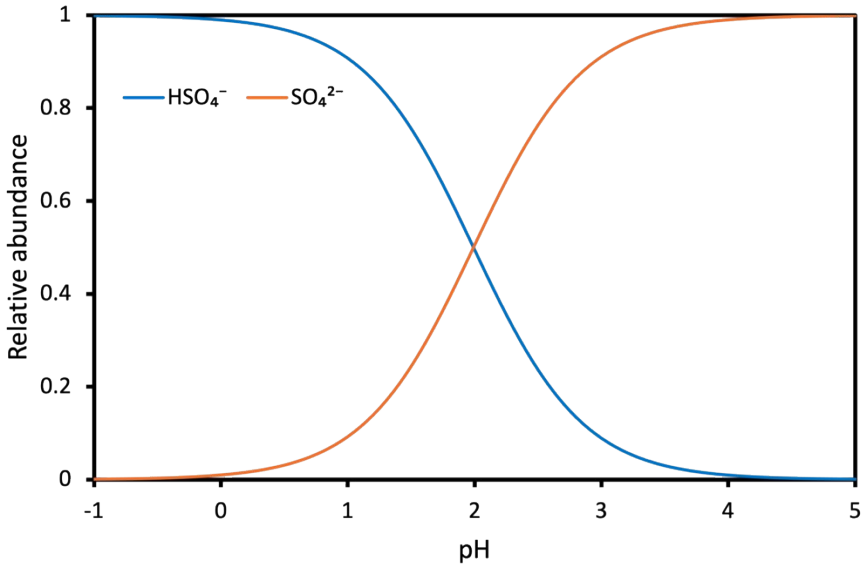

160

161 **Figure S4.** Speciation of H_2SO_4 solution as a function of *pH*.

162

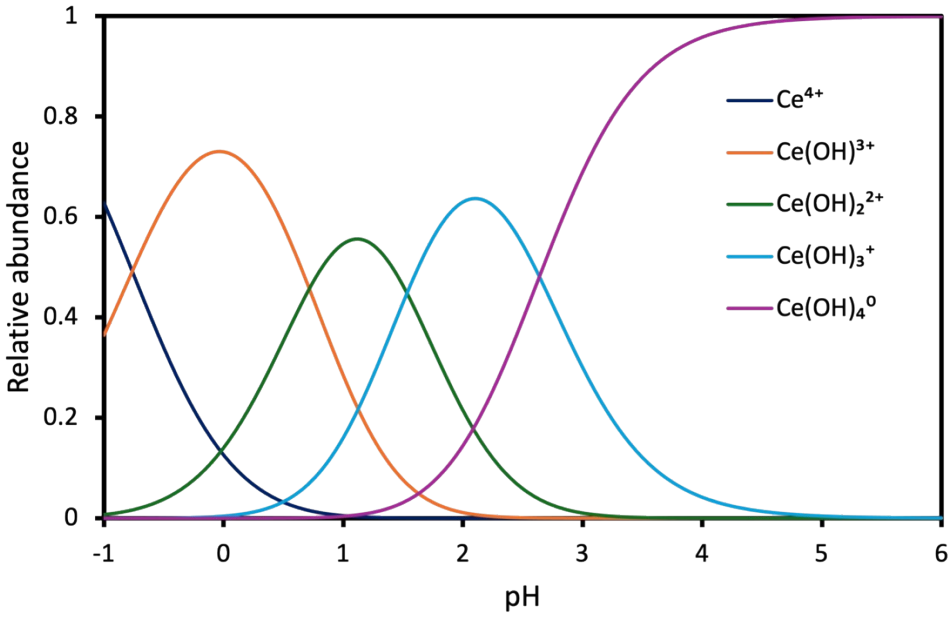

163

164 **Figure S5.** Speciation of Ce(IV) hydrolysis as a function of *pH*.

165

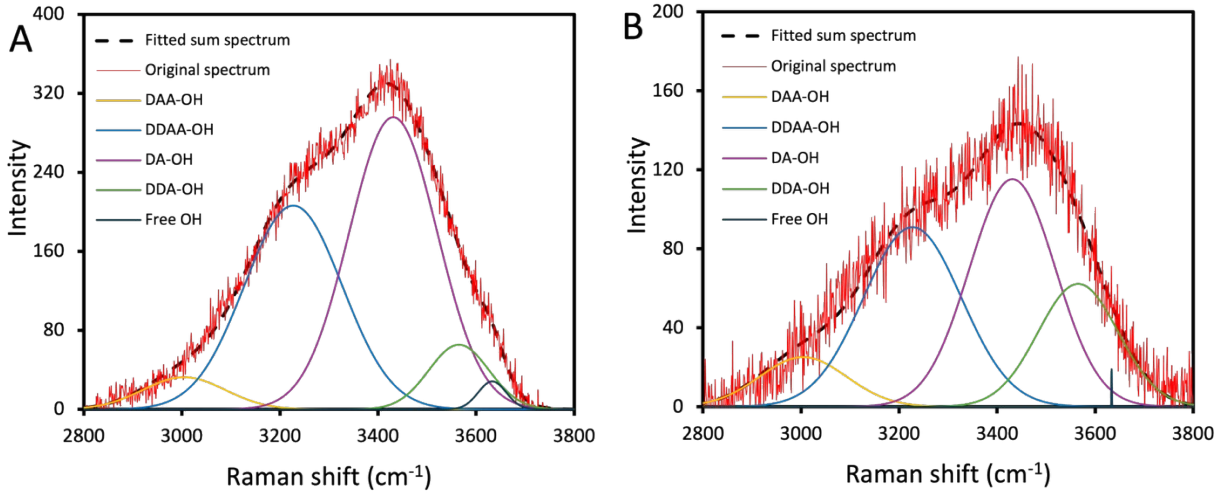

166

167 **Figure S6.** Deconvolution of high-frequency Raman spectra for 1.05 M AS (*A*), 1.23 M
168 $Ce(SO_4)_2$ in 1.05 M AS (*B*).
169

Figure S7. 0.123 M $Ce(SO_4)_2$ in water: freshly prepared (left) and six hours after preparation (right).

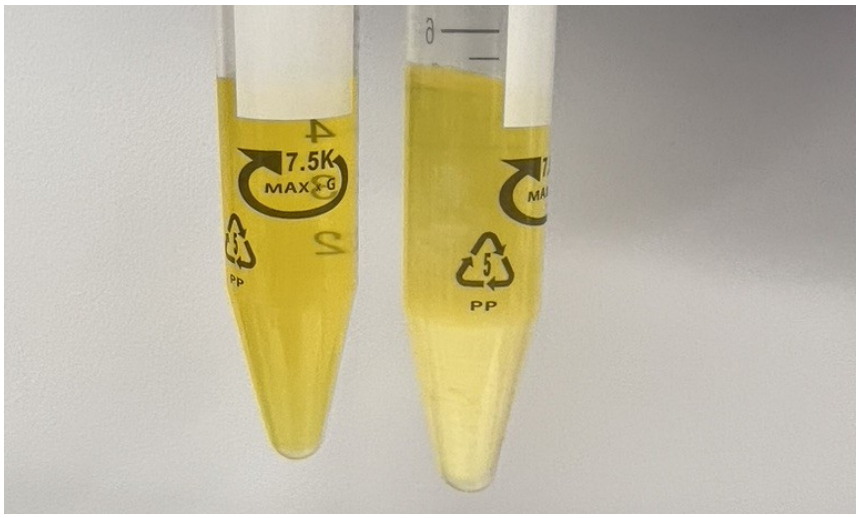

Figure S8. 0.123 M $Ce(SO_4)_2$ in 1.05 M AS: freshly prepared (left) and six hours after preparation (right).

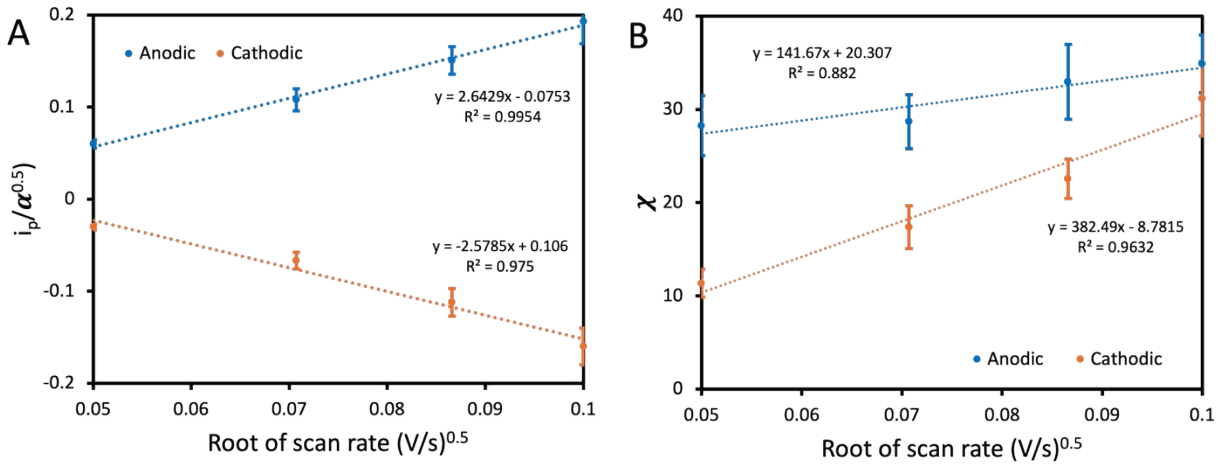

178

179 **Figure S9.** N-S (A) and K-K (B) plots of 0.123 M $Ce(SO_4)_2$ in 1.05 M AS.

180

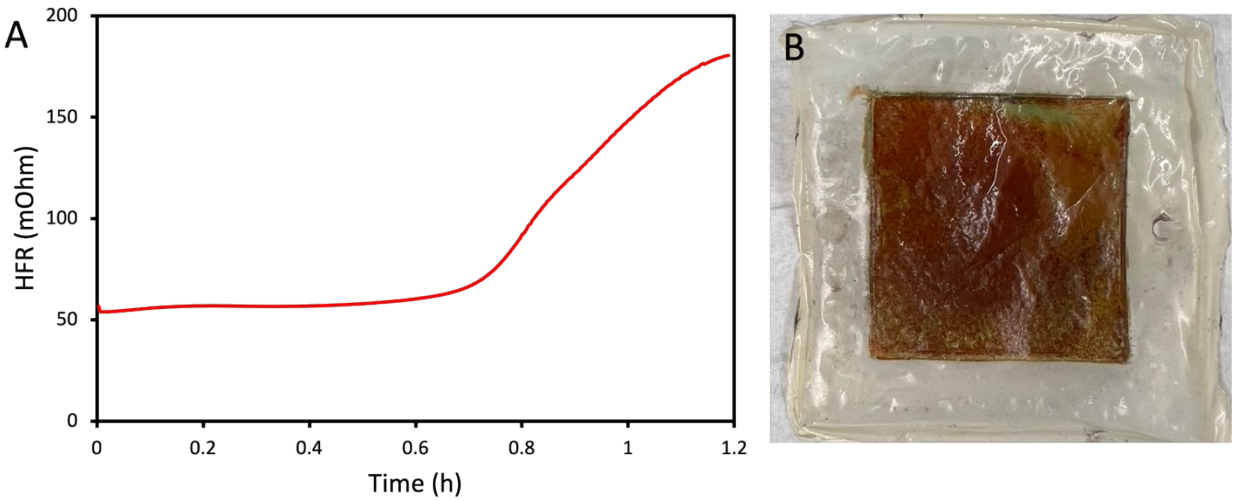

181

182 **Figure S10.** HFR curve of single charge process of V-Ti RFB (A) and membrane surface
183 deposition after the charge (B).
184

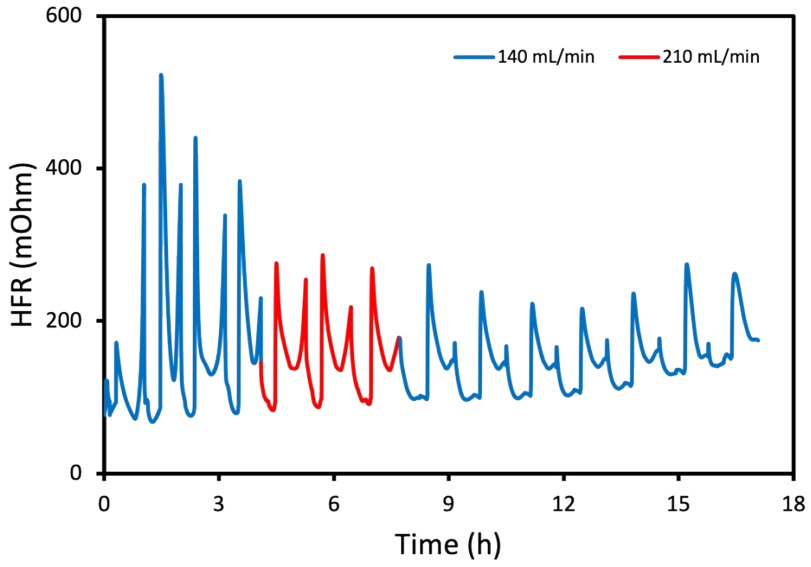

185

186 **Figure S11.** HFR curve Ti-Ce RFB applying different flow rates.

187

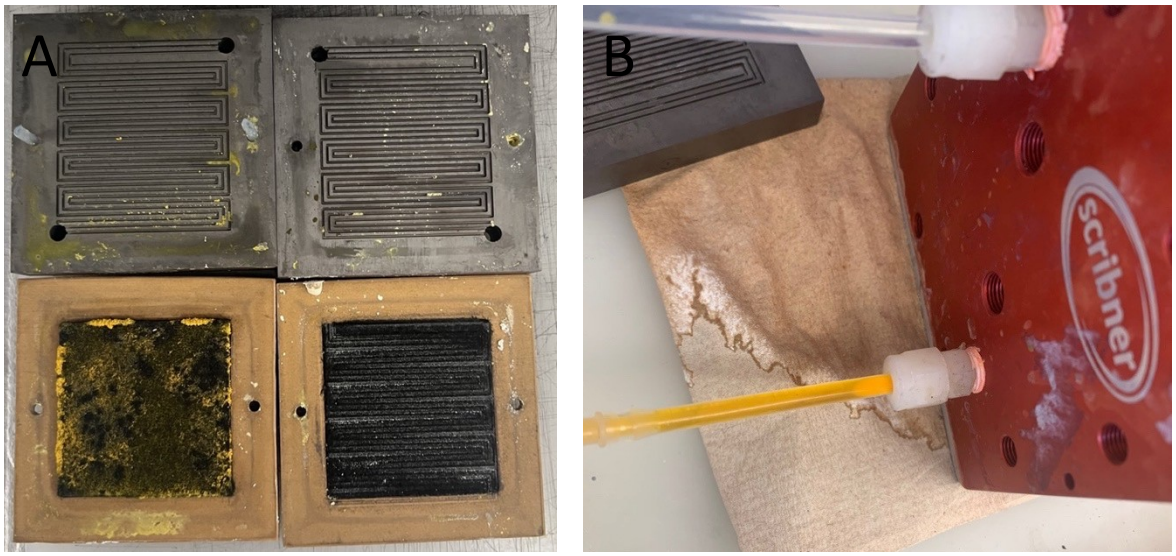

Figure S12. Ce precipitation in flow channel and electrode (A), and clogging of tube (B).

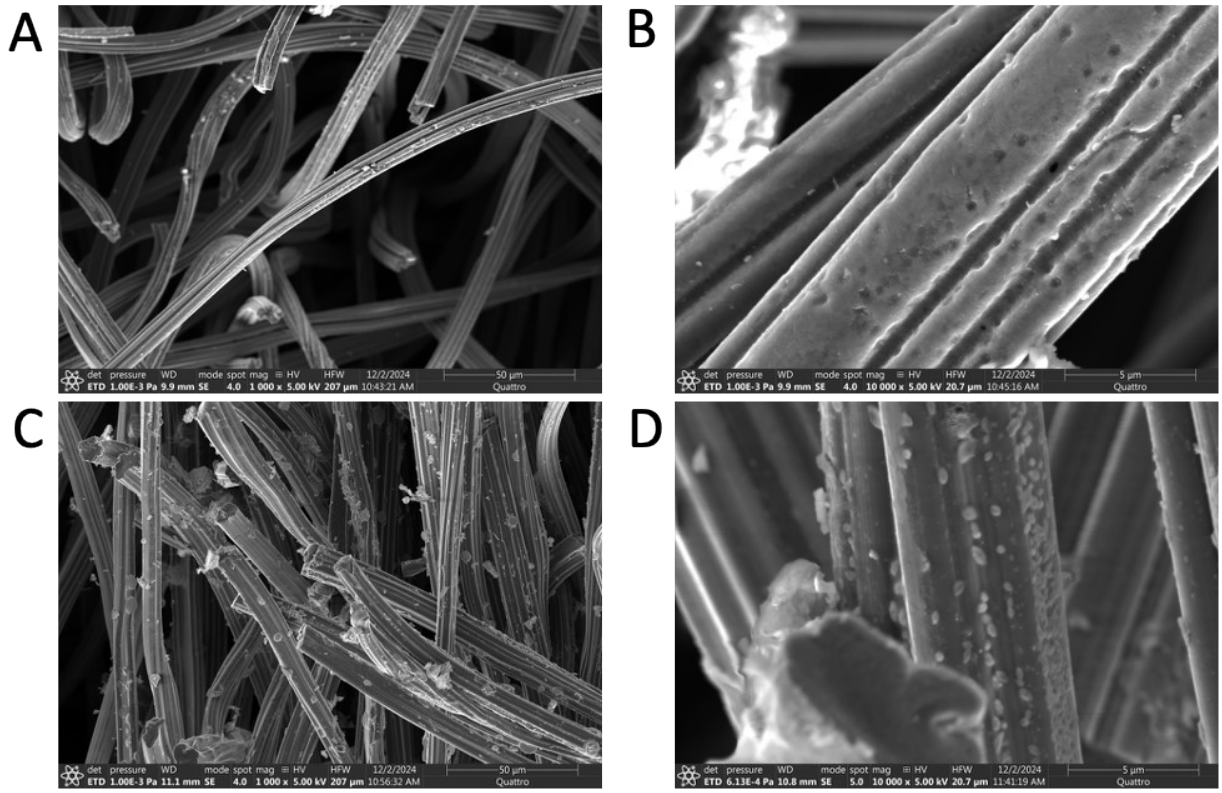

Figure S13. SEM of (*A*) and (*B*) CF before Ti-Ce RFB test, (*C*) and (*D*) CF after Ti-Ce RFB test.

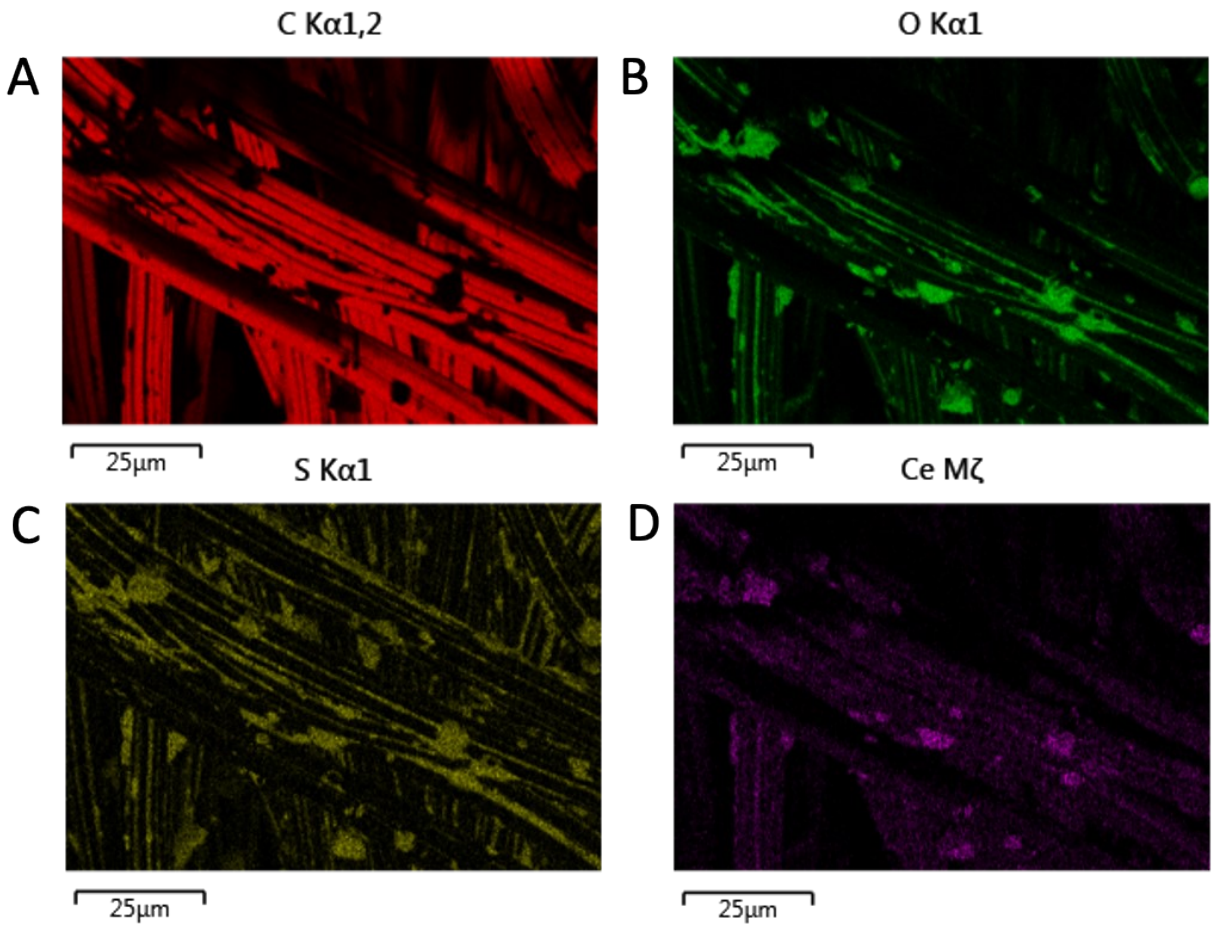

Figure S14. EDX of (*A*) carbon, (*B*) oxygen, (*C*) sulfur, and (*D*) cerium on CF after Ti-Ce RFB test.

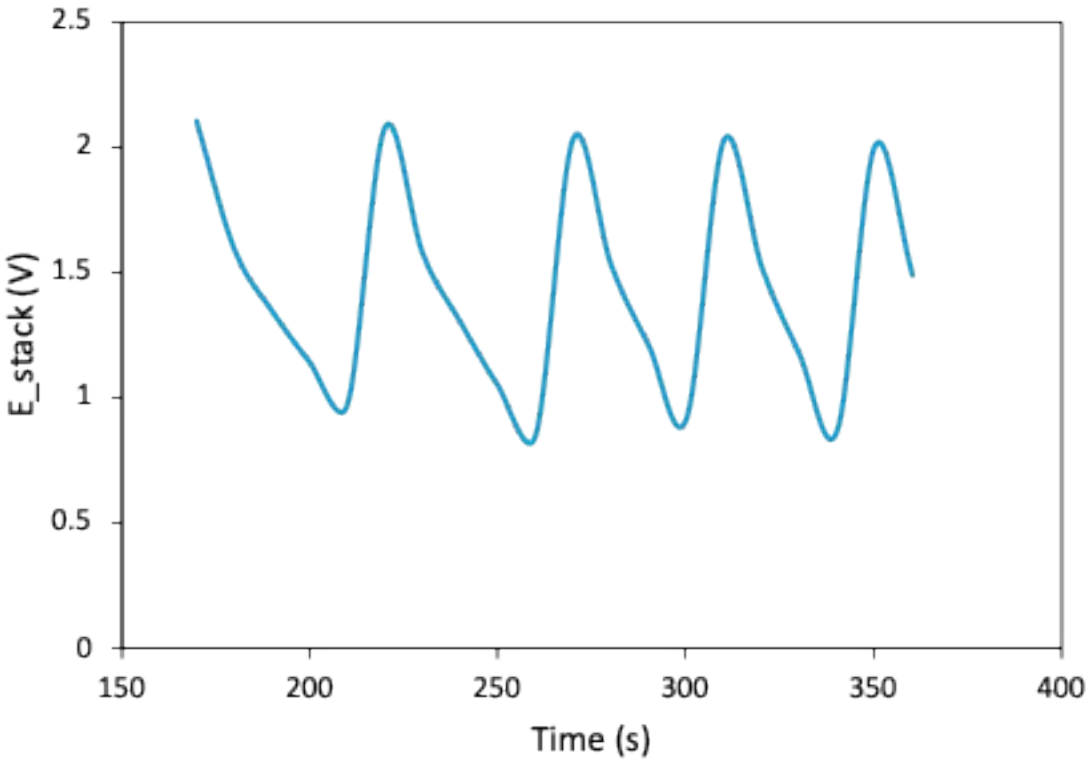

198

199 **Figure S15.** Cell voltage of Ti-Ce RFB test with conventional flow field entrance and exit design.
200

201 **Table S1** pH values of different Ce(IV) electrolytes

Sample #	Composition	pH
1	1.23 M $Ce(SO_4)_2$ in 1.05 M AS	-0.16
2	0.123 M $Ce(SO_4)_2$ in 1.05 M AS	1.63
3	0.0123 M $Ce(SO_4)_2$ in 1.05 M AS	2.60
4	1.05 M AS	5.40
5	0.123 M $Ce(SO_4)_2$ in 1.05 M H_2SO_4	-0.19
6	0.123 M $Ce(SO_4)_2$ in water	0.70
7	1.05 M H_2SO_4	-0.12

202

Table S2 Effect of Ce(IV) electrolyte on carbon paper (CP) and carbon felt (CF) in Figs. 3A and 3B

	Before immersion					After immersion				
	E_{pa} (V)	E_{pc} (V)	ΔE_p (V)	i_{pa} (mA)	i_{pc} (mA)	E_{pa} (V)	E_{pc} (V)	ΔE_p (V)	i_{pa} (mA)	i_{pc} (mA)
CP	1.278	0.949	0.329	1.92	-2.54	1.270	0.994	0.276	2.49	-2.62
CF	1.274	0.897	0.377	37.6	-14.5	1.352	0.918	0.434	37.4	-22.5

E_{pa}: anodic peak potential; E_{pc}: cathodic peak potential; ΔE_p: peak separation; i_{pa}: anodic peak current; i_{pc}: cathodic peak current.

Table S3 Electron transfer coefficient (α) calculated from Fig. 3C

Scan rate (mV/s)	α_a	α_c
2.5	0.394	0.233
5	0.302	0.233
7.5	0.262	0.218
10	0.219	0.209

α_a: anodic transfer coefficient; α_c: cathodic transfer coefficient

211 **Table S4** Electron D_0 and k_0 values of Ce cathodic reaction

Parameters	**Ce(IV) + $e^- \rightarrow$Ce(III)**
D_0 (x 10^{-4} cm^2/s)	49.2 ± 3.9
k_0 (x 10^{-4} cm/s)	24.9 ± 2.8

212

Table S5 Conductivity of Ti and Ce electrolytes

Sample	Original solution (mS/cm)	10 times diluted solution (mS/cm)
0.9 M Ce(III) in 2 M CH_3SO_3H	272.4 ± 8.6	109.4 ± 5.3
0.9 M Ti(IV) in 3.8 M CH_3SO_3H	> 9999	132.3 ± 4.1
1.23 M Ce(IV) in 1.05 M AS	261.1 ± 10.9	86.1 ± 4.9
1.23 M Ti(IV) in 1.9 M AS	247.8 ± 9.8	60.5 ± 2.6

* The conductivity of original Ti-CH_3SO_3H electrolyte was too high to be detected within the range of conductivity meter.

Table S6 Weight of CF before and after cycling test

CF	Weight (g)
Before cycling	1.3132 ± 0.0065
After cycling	2.5035 ± 0.0098

Reference

1. S. A. Hayes, P. Yu, T. J. O'Keefe, M. J. O'Keefe and J. O. Stoffer, The phase stability of cerium species in aqueous systems: I. E-pH diagram for the system. *J. Electrochem. Soc*., 2002, **149**, C623-C630.
2. B. Bouchaud, J. Balmain, G. Bonnet and F. Pedraza, pH-distribution of cerium species in aqueous systems. *J. Rare Earths*, 2012, **30**, 559-562.
3. Q. Sun, The Raman OH stretching bands of liquid water. *Vib. Spectrosc*., 2009, **51**, 213-217.
4. C. A. Buchanan, D. Herrera, M. Balasubramanian, B. R. Goldsmith and N. Singh, Unveiling the cerium(III)/(IV) structures and charge-transfer mechanism in sulfuric acid. *JACS Au*, 2022, **2**, 2742-2757.